Volume 19, Number 3, 2026. pp. 355-362

Jordan Journal of Physics

ARTICLE

Dependence of Solidification Temperature and Structural Evolution on Cooling Rate of a Platinum Nanocluster: MD Simulation Studies

Minati P. Samantaray and **Soumya S. Sarangi**

Department of Physics, Veer Surendra Sai University of Technology, Burla, 768018, India.

Doi: **https://doi.org/10.47011/19.3.7**

Received on: 30/06/2025; *Accepted on: 16/11/2025*

Abstract: Molecular dynamics (MD) simulations using a Modified Embedded Atom Method potential were conducted to understand the impact of cooling rate on the solidification temperature and structural evolution of a platinum nanocluster during solidification. The solidification temperature was calculated from the variation of potential energy with temperature at different cooling rates in the range of 10^{10} K/s – 10^{14} K/s. The solidification temperature decreased with increased cooling rate. The critical cooling rate of the nanocluster is estimated to be 1×10^{12} K/s. The evolution of atomic structures was characterized from the radial distribution function curves and common neighbor analysis. Solidification of the nanocluster is observed to initiate from the core. At the highest cooling rate, a fully amorphous structure is obtained; as the cooling rate decreases, the percentage of FCC and HCP structures increases. Even at the lowest cooling rate, no monocrystalline platinum nanocluster is observed; rather, a polycrystalline structure consisting mostly of amorphous motifs with a higher fraction of FCC and fewer HCP motifs is obtained.

Keywords: MD simulations, MEAM potentials, Platinum nanocluster, Cooling rate, Solidification temperature.

PACS Nos.: 68.35.Fx; 68.35.Ja.

1. Introduction

The unique properties of nanoparticles, already widely used or set to be used in the near future to fabricate various devices and produce new materials, have sparked considerable scientific and practical interest in the research community. They are also academically appealing because they occupy a niche between single molecules and bulk condensed phases. The properties of nanoparticles are strongly influenced by their structure as well as morphology, which is closely related to crystallization ageing [1–6]. One experimental challenge is that preparing a large ensemble of nanoparticles with a narrow size distribution is nearly impossible with current techniques. Furthermore, a distribution of structural isomers occurs even for a given particle size. To predict and control the solidification of nano-structures using different manufacturing processes, a fundamental understanding of the mechanisms of crystal nucleation and solidification is necessary. Despite the large number of experiments carried out, some unresolved issues remain, such as the dynamic aspects of phase transition and surface instabilities during the cooling process. Computer simulations are not only complementary but also necessary for structure-function relationship studies in materials. MD simulation is a prominent method for directly tracing atomic motion during phase transitions. Thus, it is widely used to characterize atomic behavior during the nucleation and growth process in various materials. For instance, Li and his group [7] examined the mechanism of surface-induced nucleation in supercooled liquid Si and Ge by using the forward flux sampling method in MD simulations. During the last two decades, several researchers have successfully used MD simulations to characterize various properties of metal nanoclusters (NCs) [8–17].

Corresponding Author: Soumya S. Sarangi **Email**: sssarangi_phy@vssut.ac.in

The morphology of NCs plays a vital role in determining their properties. Various structural modifications such as icosahedral, decahedral, polycrystalline, and amorphous structures are observed in NCs synthesized by high-temperature techniques, e.g. evaporation and aerosol methods [18, 19], so nucleation occurs spontaneously. Therefore, understanding the impact of cooling rate on phase transitions is necessary to characterize solidification phenomena. During the last decade, researchers have extensively studied the effect of cooling rate on solidification of many metal NCs using MD simulations. Shibuta *et al.* [20, 21] investigated via MD simulations the influence of cooling rate and size on the structural and thermal properties of molybdenum nanoparticles and revealed that the structure of the NCs varied from BCC single-crystalline at lower cooling rates (~10^{10} K/s) to glassy at higher cooling rates (~10^{13} K/s) and polycrystalline at intermediate cooling rates (~10^{12} K/s). They also showed that the solidification points of the NCs decreased with increased cooling rate and dropped abruptly at the 10^{12} K/s order of magnitude (critical cooling rate). Similar investigations have been carried out on FCC metal NCs, such as nickel [22, 23], gold [22, 24], and copper [23, 25]. Domekeli et al. have shown that the solidification behavior of palladium nanoparticles differs depending on their cooling rate [26]. The critical cooling rates of cobalt melt and silver nanoparticles are reported to be 1×10^{11} K/s and 2×10^{12} K/s, respectively [27, 28]. In an interesting study, Abdeslam and Chihi explored the effect of cooling rate on the physical properties of niobium NCs [29]. Recently, the microstructural evolution of copper, nickel and silver NCs during the crystallization process at various cooling rates was characterized by our group. We found that below their respective critical temperatures, the NCs possessed amorphous/glassy structures, and above them, they acquired polycrystalline structures [30]. These findings contribute to the broader understanding of size-dependent thermodynamic properties and the role of cooling rates in shaping the structure of NCs.

Platinum (Pt) is one of the important noble metals; Pt nanoparticles are used in various industries. The electronics industry uses Pt for hard disks and thermocouples. It is also used to manufacture optical fibres and LCDs, spark plugs, turbine blades, etc. Despite these potential uses, research on Pt NC remains scarce. To our knowledge, no research on the effect of cooling rate on the atomic structure of Pt NC has been done. Therefore, to regulate, improve, and broaden its applicability, detailed structural insight is needed. In this study, the structural evolution of a platinum nanocluster with varying cooling rates is analyzed by MD simulations using a Modified Embedded Atom Method (MEAM) potential. The NC structure is examined by analyzing atomic configurations using radial distribution functions and the Common Neighbor Analysis method. The solidification temperature for each cooling rate is obtained from the caloric curve, and the fractions of various structural motifs are quantified at different cooling rates.

2. Simulation Details

FCC Pt crystal with a box length of 31.36 Å and composed of 2048 atoms is generated by employing periodic boundary conditions (PBC) along all three dimensions. The crystal bulk is equilibrated for a period of 1 ns at 300 K in the constant-volume canonical ensemble (NVT) and subsequently heated to 3000 K (well above the melting temperature of the Pt crystal) in the constant-pressure canonical ensemble (NPT) to achieve the molten state, followed by equilibration of 1 ns in NVT conditions at 3000 K. The melting temperature of the bulk Pt crystal is estimated to be ~2100 K, which is in fair agreement with the experimental value of 2040 K [31] (this validates the potential model used). The PBCs are then removed in the melted bulk system in order to achieve the free-standing nanocluster (Pt NC). The molten Pt NC is quenched to 300 K at 10^{12} K/s and then equilibrated at 300 K for 1 ns in the NVT ensemble to obtain a stable NC. To investigate the effect of cooling rate on the microstructures of the NC, the NC is reheated to 2000 K at 10^{12} K/s. It is then equilibrated for 1 ns at 2000 K, and the equilibrated structures are treated as the starting point for the rate-dependent cooling process. Subsequently, the NC is cooled from the high temperature (2000 K) to room temperature (300 K) at various cooling rates from 10^{10} K/s to 10^{14} K/s.

MD simulations have been conducted using the Large-Scale Atomic/Molecular Massively Parallel Simulator (LAMMPS) program [32]. Newton's equation of motion has been solved

using the velocity-Verlet algorithm [33, 34] with a time step of 1 fs. The system temperature is regulated using the Nose-Hoover thermostats [35]. Baskes MEAM potentials are used for the interatomic interactions [36–38]. MEAM is the modified form of the Embedded-Atom-Method (EAM) potentials [39, 40]. The MEAM formulation includes a local electron density term that is angle-dependent, capturing the directional bonding nature of FCC. The total energy for a system in the MEAM formalism is obtained as:

$$V(r_i) = \sum_i^N F(\rho_i) + \sum_{i \neq j} S_{ij}\, \phi_{ij}(r_i - r_j) \qquad (1)$$

where $F(\rho_i)$ denotes the embedding energy for embedding the atom into a local site having electron density ρ_i, φ_{ij} represents the pair interaction term ~~among~~ between atoms i and j, and S_{ij} stands for the screening function. The total number of atoms is denoted by N. The detailed formalism of the model is given in the literature [36]. The potential parameters ~~employed~~ used in the present work ~~have been~~ are listed in Table 1. The open visualization tool OVITO has been used for the visualization of atomic structures [41].

TABLE 1. MEAM Potential parameter.

	E_i^0	R_i^0	α_i	A_i	β_i^0	β_i^1	β_i^2	β_i^3	t_l^0	t_l^1	t_l^2	t_l^3
Pt	5.77	3.92	6.442	1.04	4.673	2.20	6	2.2	1	2.733	1.373	2.953

3. Results and Discussion

3.1. Estimation of Solidification Point

One of the most important methods for detecting the melting/solidification temperature of materials is monitoring the variation of average potential energy with temperature. This variation curve is referred to as the caloric curve. Theoretically, in a first-order phase transition, the temperature at which enthalpy changes discontinuously reflects the distinct atomic-order characteristics of solid and liquid phases and is commonly denoted as the melting or solidification point during heating or cooling, respectively. First-order phase transitions can also be characterized by a sudden and discontinuous change in energy, specific heat, self-diffusion coefficients, etc. Fig. 1 illustrates the variation of average potential energy per atom of the Pt NC during the cooling process at different cooling rates. The inset shows the variation of average potential energy per atom during heating, and the melting point is estimated from the temperature at which the curve shows a sharp jump. The melting temperature of Pt NC is estimated to be ~1300 K, which is much lower than the crystal's melting temperature (~2100 K). During cooling, the potential energy initially decreases linearly as temperature decreases, then drops abruptly at a specific temperature (i.e., the solidification temperature), and then resumes a linear decrease at the lower cooling rates of 1×10^{10} K/s and 2×10^{10} K/s. This abrupt fall in potential energy indicates a first-order phase transition from liquid to solid (crystallized) state. However, for the cooling rates 1×10^{11} K/s and 1×10^{12} K/s, the temperature range over which the transition occurs becomes wider, and estimating the solidification temperature (T_c) becomes challenging. For higher cooling rates (5×10^{12} K/s and higher), the potential energy decreases monotonically with decreasing temperature, indicating the lack of formation of a crystallized state, and hence, T_c could not be estimated.

Consequently, the cooling rate 1×10^{12} K/s is considered as the critical cooling rate (R_c) of the studied Pt NC. R_c is defined as the minimum cooling rate required to facilitate crystallization in materials. Hence, it is a crucial parameter for regulating the material structure. The estimated R_c in this work is consistent with those reported for other metallic NCs [21, 28, 30]. However, it should be noted that critical cooling rates are sensitive to the size of the NCs.

Table 2 provides the estimated T_c for the NCs at various cooling rates, and Fig. 2 shows the same information graphically. An error bar of ±5 K is added to the estimated T_c to incorporate the statistical error that might have occurred in the force calculations due to the small size of the NC. The solidification temperature of the NC is sensitive to cooling rate and decreases as the cooling rate increases. The detailed structures of the solidified NC under various cooling rates are characterized by using the radial distribution function and Common Neighbor Analysis.

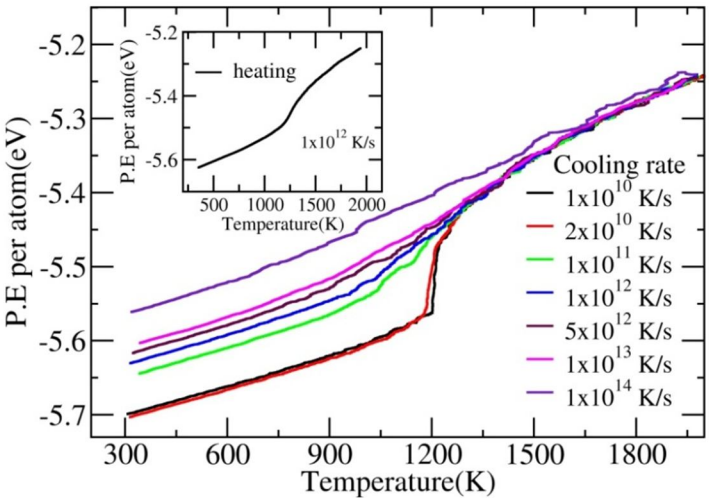

FIG. 1. The variation of average potential energy per atom versus temperature for Pt NC at various cooling rates during the cooling process. The inset shows the same but during the heating process.

TABLE 2. Solidification temperature of Pt NC with respect to cooling rate.

Cooling rate (K/s)	Solidification Temperature
1×10^{10}	1200 ±5 K
2×10^{10}	1180 ±5 K
1×10^{11}	1050 ±5 K
1×10^{12}	980 ±5 K
5×10^{12}	---
1×10^{13}	---
1×10^{14}	---

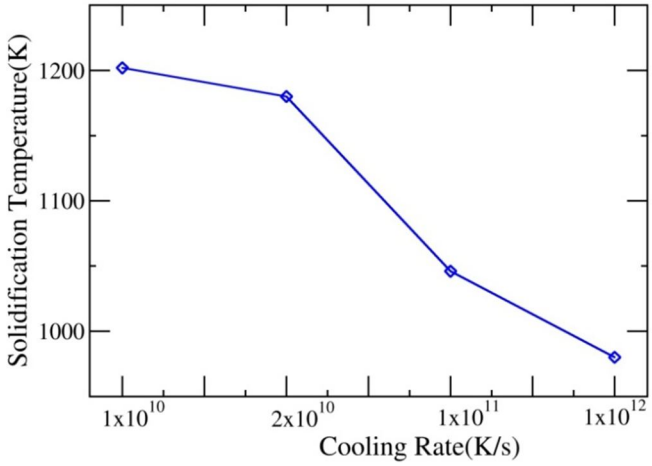

FIG. 2. Solidification temperature of Pt NC with respect to various cooling rates.

3.2. Structural Analysis using Radial Distribution Function

A key technique for identifying solid-liquid/liquid-solid phase transitions and gaining insight into atomic arrangements involves the examination of the radial distribution function (RDF) at pertinent temperatures. The RDF provides valuable information about the spatial distribution of atoms, offering a detailed understanding of the structural transformations that occur as the NCs undergo phase changes. This method is a powerful tool to unravel the dynamic and intricate nature of atomic arrangements during the thermal evolution of nanoscale systems. The RDF of a system is given by:

$$g(r)=\frac{V}{N}\frac{n(r)}{4\pi r^2 \Delta r} \quad (2)$$

where V represents the volume of the system, N denotes the total number of atoms in the system, and $n(r)$ signifies the count of atoms within the width Δr at a specific radius (r) from the atom. Fig. 3 presents the results of RDF analysis for the solidified NC (at 300 K) at various cooling rates.

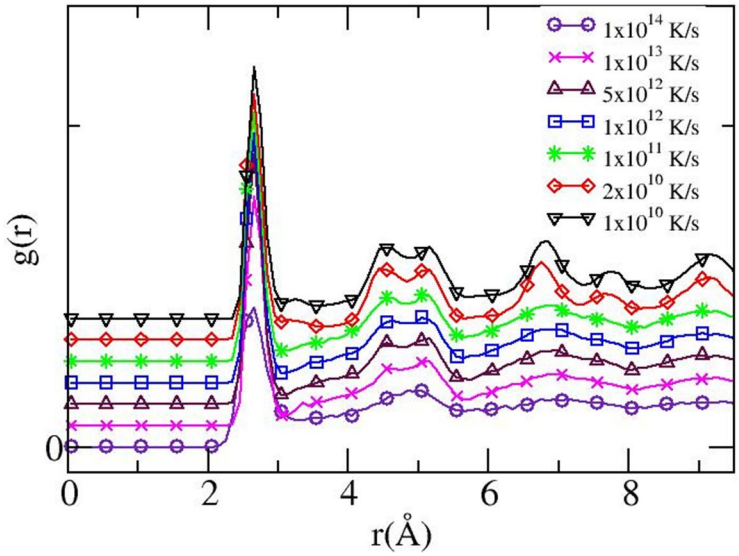

FIG. 3. RDF curves of solidified (at 300 K) of Pt NC at various cooling rates.

The impact of cooling rate on the structure of solidified NC is clearly evident in the graphical representations. Sharp peaks indicative of long-range order are observed at lower cooling rates (below the critical cooling rate). The peak locations align with the corresponding FCC Pt-structure at 300 K, suggesting that when quenched slowly (with a rate below R_c), the melted NC transforms into more crystal-like structures. However, for the smallest cooling rate studied (1×10^{10} K/s), a sharp first peak, a flat and bifurcated second peak, and a few other smaller higher-order peaks are observed, which indicates a polycrystalline structure rather than a monocrystalline FCC structure. As the cooling rate increases, all peaks become broader and smaller, indicating short-range ordering. For cooling rates above R_c, all peaks except the first and second vanish. This clearly indicates a pure amorphous structure of the NC. The RDF profiles highlight the shift from long-range ordering characteristic of crystalline structures to short-range ordering characteristic of glassy or amorphous configurations, offering valuable insight into the structural transformations that occurred during the cooling processes.

3.3. Structural Information from Common Neighbour Analysis

RDF analysis provides estimates whether the structure is crystalline or amorphous. However, precise characterization of the crystal structure requires additional tools. The Common Neighbor Analysis (CNA) technique serves as a standard tool for characterizing the local structure of solid materials. CNA is seamlessly integrated into OVITO software, which was used to perform the analysis. Combining the RDF and CNA methods enables a more detailed understanding of the material's structural characteristics, allowing for a thorough exploration of structural configurations. The CNA method encodes n-body clusters using their common neighbor relationships and uses their relative abundances to characterize structural order in nanoparticles. This method characterizes the local environment of a central atom [42, 43]. The atomic structure of the NC at various stages (melted/2000 K, at the solidification point, solidified/300 K) during the cooling process at different cooling rates is depicted in Fig. 4. Notably, it is observed that the absence of periodic boundary conditions prevents the identification of all surface atoms in their respective structures. From the atomic structures, the percentage of various motifs (FCC, HCP or amorphous) is obtained with the help of CNA using the OVITO program. The CNA analysis reveals that at 2000 K, the NC is fully amorphous. As the temperature decreases during cooling at lower cooling rates (below Rc), the amorphous percentage decreases and the crystalline percentage increases.

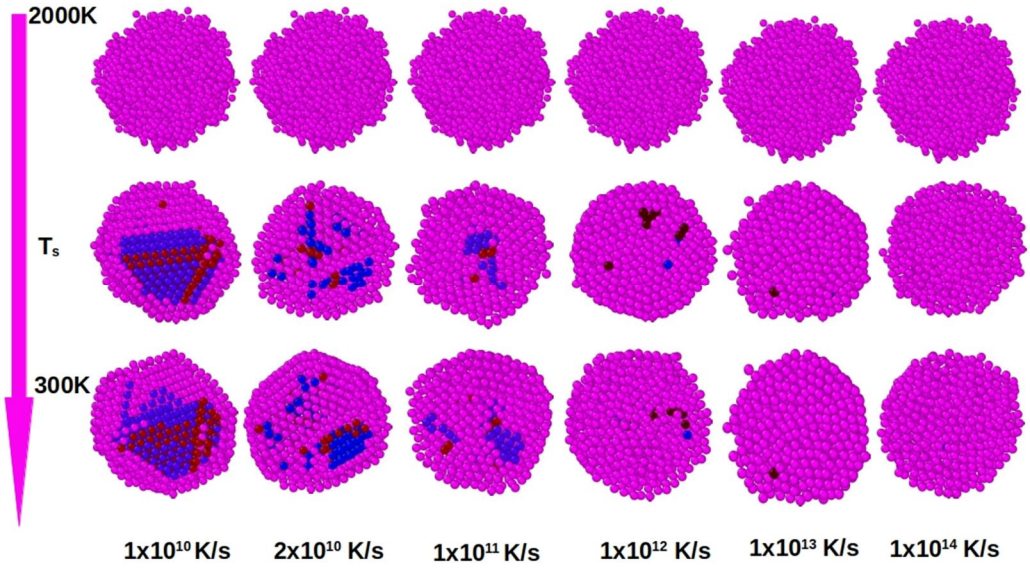

FIG. 4. Snapshots of the Pt NC during the solidification process at various cooling rates, analyzed by the CNA method. The color code used is: pink-amorphous; blue-FCC; maroon-HCP.

As expected, for higher cooling rates, the solidified NC contains almost no crystalline phases and is fully amorphous. Even at the lowest cooling rate studied (1×10^{10} K/s), the solidified NC is not fully crystallized but is polycrystalline in nature (as seen from the radial distribution function analysis). It contains both amorphous (dominant) and crystalline phases (FCC, HCP). Among the crystalline phases, FCC is dominant. The influence of cooling rate becomes evident from the solidification point onward and becomes particularly pronounced towards the end of the cooling process. Moreover, it is interesting to observe directly that solidification nucleates from the core of the NC. The crystallized NC is observed to have a crystal core and an amorphous shell. This supports the idea that solidification of the NCs occurs through a nucleation and growth process. The undercooling effect of solidification plays a key role, as it provides the necessary thermodynamic force for the liquid to transform into a solid. Once a sufficient degree of undercooling occurs, a group of atoms at the center acts as a site for a nucleus to form, and then the growth proceeds from the center to the surface. Surface melting is a well-known phenomenon in nanoparticles, and this work predicts that solidification, in contrast to melting, initiates from the core.

This comprehensive analysis provides valuable insight into the complex interplay between cooling rates and the resulting atomic structures, shedding light on the unique phases and arrangements exhibited by the system during the cooling process. Hence, with lower cooling rates, the formation of polycrystalline structures is favored and higher cooling rates promote the development of amorphous or glassy structures. Although the initial structure was FCC, the solidified NC obtained for the lower cooling rates contained FCC and HCP structures. The percentage of both motifs increases as the cooling rate decreases, with FCC becoming dominant at lower cooling rates. Table 3 lists the fraction of atoms acquiring different crystal structures in the solidified NC for all studied cooling rates. Fig. 5 represents the data graphically for a better understanding.

TABLE 3. Number of atoms having amorphous, FCC, and HCP structures at different cooling rates in solidified (300 K) Pt NCs.

Rate (K/s)	Amorphous	FCC	HCP
1×10^{10}	1308	526	214
2×10^{10}	1380	505	163
1×10^{11}	1850	106	92
1×10^{12}	1990	36	22
5×10^{12}	2040	3	5
1×10^{13}	2047	0	1
1×10^{14}	2048	0	0

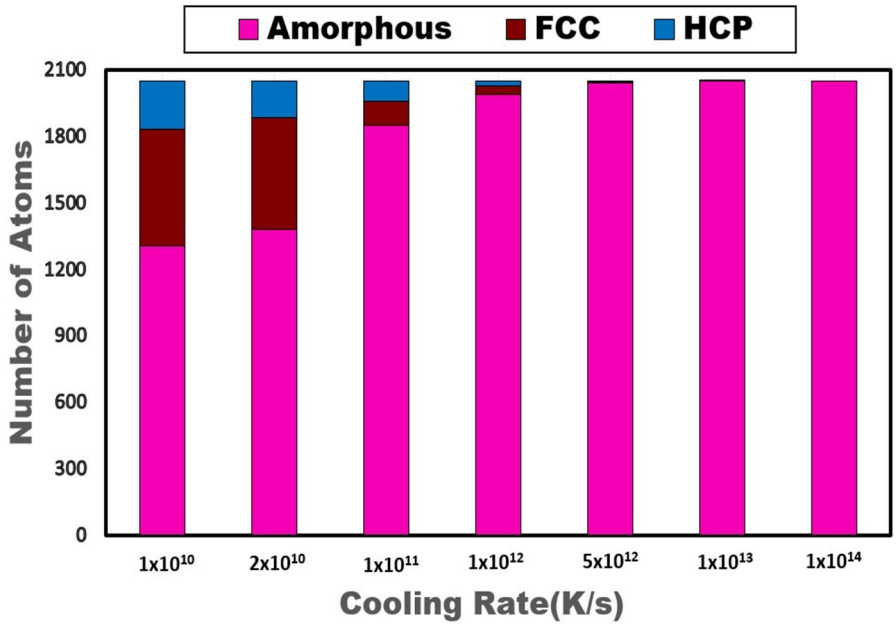

FIG. 5. Number of atoms having amorphous, FCC, and HCP structures in solidified Pt NCs.

4. Conclusion

To summarize, MD simulations have been carried out to examine the dependence of solidification temperature and atomic structure of a platinum nanocluster (containing 2048 atoms) on cooling rate during the solidification process. The study suggests that the atomic structure of the nanocluster is strongly influenced by the formation conditions. The critical cooling rate, below which the melted nanocluster acquires a polycrystalline structure, has been estimated to be 1×10^{12} K/s. The solidification temperature decreases as the cooling rate increases. The polycrystalline structure is found to be a mixture of mostly amorphous motifs with crystalline FCC and HCP structures. Moreover, it is interesting to observe the solidification initiating from the core of the nanocluster, which is attributed to the undercooling phenomenon of atoms in metal nanoparticles. As predicted by thermodynamics and kinetics, it is found that slow cooling favors the formation of polycrystalline phases, while fast cooling results in the formation of more amorphous structures. We propose that a single crystalline structure may be obtained at lower cooling rates than those studied here, but this is computationally expensive. In view of real experimental conditions at finite temperatures, these findings provide useful guidance for various applications of the platinum nanocluster, as it is still not straightforward to control atomic configurations of nanoparticles experimentally. The work may be extended with larger-sized nanoclusters and lower cooling rates to obtain further insights.

Acknowledgement

The authors thank “Odisha State Higher Education Council (Letter No. 191/144(pt)/ OSHEC-2022-23), OURIIP-2022 seed fund scheme” for supporting the research work.

Declaration of Interest

The authors declare no competing interests.

References

[1] Wu, D.T., Granasy, L., and Spaepen, F., MRS Bull., 29 (2004) 945.

[2] Li, T., Donadio, D., Chiringhelli, L.M., and Galli, G., Nature Mater., 8 (2009) 726.

[3] Barik, S. and Sarangi, S.S., Mater. Proc., 56 (1) (2022) 60.

[4] Sarangi, S.S., Mater. Proc., 41 (2) (2021) 413.

[5] Barik, S. and Sarangi, S.S., Molecular Simulation, 49 (4) (2023) 377.

[6] Barik, S., Bhramarjal, C., and Sarangi, S.S., Jordan J. Phys., 17 (4) (2024) 461.

[7] Asta, M., Beckermann, C., Karma, A., Kurz, W., Napolitano, R., Plapp, M., Purdy, G., Rappaz, M., and Trivedi, R., Acta Mater., 57 (2009) 941.

[8] Shibuta, Y., Watanabe, Y., and Suzuki, T., Chem. Phys. Lett., 475 (2009) 264.

[9] Watanabe, Y., Shibuta, Y., and Suzuki, T., ISIJ Int., 50 (2010) 1158.

[10] Sarangi, S.S., Satyam, P.V., Nayak, S.K., and Mahanti, S.D., Indian J. Phys., 91 (2017) 853.

[11] Samantaray, M.P. and Sarangi, S.S., Indian J. Phys., 96 (2022) 2285.

[12] Qiao, Z., Feng, H., and Zhou, J., Phase Transit., 87 (2013) 59.

[13] Samantaray, M.P. and Sarangi, S.S., Int. J. Adv. Sci. Eng., 6 (2020) 18.

[14] Samantaray, M.P. and Sarangi, S.S., Int. J. Nanosci., 22 (01) (2023) 2250052.

[15] Nguyen, N.H., Henning, R., and Wen, J.Z., J. Nanopart. Res., 13 (2011) 803.

[16] Samantaray, M.P. and Sarangi, S.S., Mater. Today, Proc., 46 (2021) 10861.

[17] Sarangi, S.S., In: Selected Articles from the 2nd International Conference on Advanced Nanomaterials and Applications (ICANA 2024), (Springer Proceedings in Physics, 2025), Vol. 413, pp. 221– 227.

[18] Tehuacanero, S., Herrera, R., Avalos, M., and Yacamán, M.J., Acta Metall. Mater., 40 (1992) 1663.

[19] Magnusson, M.H., Deppert, K., Malm, J.-O., Bovin, J.-O., and Samuelson, L., Nanostruct. Mater., 12 (1999) 45.

[20] Shibuta, Y., J. Therm. Sci. Technol., 7 (2012) 45.

[21] Shibuta, Y. and Suzuki, T., Chem. Phys. Lett., 502 (2011) 82.

[22] Shibuta, Y. and Suzuki, T., Chem. Phys. Lett., 498 (2010) 323.

[23] Nguyen, T.D., Nguyen, C.C., and Tran, V.H., RSC Adv., 7 (2017) 25406.

[24] Shim, J.-H., Lee, S.-C., Lee, B.-J., Suh, J.-Y., and Cho, Y.W., J. Cryst. Growth, 250 (2003) 558.

[25] Chen, F.F., Zhang, H.F., Qin, F.X., and Hu, J.Q., J. Chem. Phys., 120 (2004) 1826.

[26] Domekeli, U., Sengul, S., and Celtek, M., International Scientific Conference, "UNITECH", (2018), GABROVO.

[27] Sun, H., Jian, Z., Xu, J., Jiang, B., and Liu, C., Journal of Thermal Analysis and Calorimetry, 138 (2019) 287.

[28] Quoc Vo, T. and Kim, B., Eur. Phys. J. D, 73 (2019) 183.

[29] Abdeslama, S. and Chihi, T., Chinese Journal of Physics, 56 (2018) 2710.

[30] Samantaray, M.P. and Sarangi, S.S., Physica Scripta, 98 (2023) 125971.

[31] Bezemer, J. and Jongerius, R.T., Physica B+C, 83 (3) (1976) 338.

[32] Plimpton, S.J., J. Comput. Phys., 117 (1995) 1.

[33] Allen, M.P. and Tildesley, D.J., "Computer Simulation of Liquid", (Oxford University, 1997).

[34] Nose, S., Journal of Physics: Cond. Matter, 2 (1990) SA115–A.

[35] Hoover, W.G., Phys. Rev. A, 31 (1985) 1695.

[36] Baskes, M.I., Phys. Rev. B, 46 (1992) 2727.

[37] Baskes, M.I. and Johnson, R.A., Modell. Simul. Mater. Sci. Eng., 2 (1994) 147.

[38] Baskes, M.I., Mater. Chem. Phys., 5 (1997) 152.

[39] Daw, M.S. and Baskes, M.I., Phys. Rev. B, 29 (1984) 6443.

[40] Daw, M.S., Baskes, M.I., Phys. Rev. Lett., 50 (1983) 1285.

[41] Stukowski, A., Model. Simul. Mater. Sci. Eng., 18 (2009) 015012.

[42] Honeycutt, J.D. and Andersen, H.C., J. Phys. Chem., 91 (19) (1987) 4950.

[43] Faken, D. and Jónsson, H., Comput. Mater. Sci., 2 (2) (1994) 279.